Nb_3Sn superconducting radiofrequency cavities: fabrication, results, properties, and prospects

2017 Supercond. Sci. Technol. 30 033004

(http://iopscience.iop.org/0953-2048/30/3/033004)

Operated by Fermi Research Alliance, LLC under Contract No. DE-AC02-07CH11359 with the United States Department of Energy.

OPEN ACCESS
IOP Publishing
Superconductor Science and Technology
Supercond. Sci. Technol. **30** (2017) 033004 (17pp)
doi:10.1088/1361-6668/30/3/033004

Topical Review

Nb_3Sn superconducting radiofrequency cavities: fabrication, results, properties, and prospects

S Posen[1,3] **and D L Hall**[2]

[1] Fermi National Accelerator Laboratory, Batavia, IL 60510, USA
[2] Cornell Laboratory for Accelerator-Based Sciences and Education, Ithaca, NY 14853, USA

E-mail: sposen@fnal.gov and dlh269@cornell.edu

Received 1 August 2016
Accepted for publication 16 November 2016
Published 23 January 2017

Abstract

A microns-thick film of Nb_3Sn on the inner surface of a superconducting radiofrequency (SRF) cavity has been demonstrated to substantially improve cryogenic efficiency compared to the standard niobium material, and its predicted superheating field is approximately twice as high. We review in detail the advantages of Nb_3Sn coatings for SRF cavities. We describe the vapor diffusion process used to fabricate this material in the most successful experiments, and we compare the differences in the process used at different labs. We overview results of Nb_3Sn SRF coatings, including CW and pulsed measurements of cavities as well as microscopic measurements. We discuss special considerations that must be practised when using Nb_3Sn cavities in applications. Finally, we conclude by summarizing the state-of-the-art and describing the outlook for this alternative SRF material.

Keywords: superconducting cavities, niobium–tin, particle accelerators, superconducting thin films, superconducting materials

(Some figures may appear in colour only in the online journal)

1. Introduction

Niobium has properties that make it extremely useful in superconducting radiofrequency (SRF) cavities, such that it is by far the material of choice for modern SRF accelerators [1–7]. Over years of development, researchers have pushed the performance of niobium cavities, overcoming a number of non-fundamental limitations—see overview of development in [8, 9] and [10–14] for examples of mitigation: multipacting, field emission, high field Q-slope—and now cavities are being produced that reach close to the fundamental limits of this material. To continue to increase the reach of particle accelerators for frontier scientific research and to open new industrial applications for accelerators, researchers are examining the potential of alternatives to niobium with superior SRF properties.

Two key figures of merit that are used to evaluate SRF cavities are accelerating electric field (E_{acc}) and quality factor (Q_0). Q_0 is a measure of the efficiency of the cavity. The higher the Q_0, the lower the power dissipated (P_{diss}) in the walls of the cavity,

$$P_{diss} = \frac{(E_{acc}L)^2}{\frac{R}{Q}Q_0}, \quad (1)$$

[3] Author to whom any correspondence should be addressed.

where L is the length of the cavity and $\frac{R}{Q}$ is a parameter dependent only on the cavity geometry[4]. Q_0 is strongly dependent on temperature and on the properties of the superconductor. E_{acc} determines the length of accelerator required to bring a particle beam up to a given energy. E_{acc} is proportional to the peak surface magnetic field, H_{pk}, which generally is the cause of limitation in state-of-the-art niobium cavities—even for an ideal defect-free surface, once H_{pk} reaches the superheating field H_{sh}, flux penetrates the superconductor [15–18]. Due to the high frequency of the applied fields, flux would enter and leave the superconductor billions of times per second, creating substantial dissipation. This can quickly cause overheating and 'quench' of superconductivity. Niobium cavities treated with modern surface preparation methods can reach H_{pk} very close to the H_{sh} of niobium.

Q_0 can be defined by the surface resistance (R_s) by $Q_0 = \frac{G}{R_s}$, where G is a parameter dependent on cavity geometry[5]. R_s can further be broken down into a temperature dependent component R_{BCS} and a temperature independent component R_{res}:

$$R_s(T, H_{pk}) = R_{BCS}(T, H_{pk}) + R_{res}(H_{pk}). \quad (2)$$

From BCS theory, the surface resistance can be approximated as:

$$R_{BCS} = A\frac{f^2}{T}\exp\left(-\frac{\Delta}{k_b T}\right). \quad (3)$$

Residual resistance is the component of surface resistance that remains at low temperature, where R_{BCS} is exponentially small. Potential sources for R_s include trapped magnetic flux, moving flux lines, and impurity heating.

Modest gains in E_{acc} and R_s can continue to be made through modification of cavity shapes [19, 20] and surface preparation. Alternative superconductors require more development than these efforts, but they offer a way to significantly increase performance beyond the fundamental limits of niobium. An overview of the different materials being considered for SRF applications is given in [21], but one especially promising material is Nb_3Sn. It offers both a large critical temperature (T_c as high as 18 K) and large predicted H_{sh}, both of which are approximately twice those of niobium [8, 22]. A large H_{sh} is attractive for future high energy accelerators, as cavities reaching H_{pk} close to this field would greatly decrease the overall length and cost. A large T_c offers two ways to improve cryogenic efficiency, which are illustrated in figure 1: (1) strong suppression of R_{BCS} for a given operating temperature; and (2) the possibility of operation at higher temperatures, where cryogenic plant efficiency is far higher than for typical niobium operating temperatures ~2 K [23]. Both of these factors reduce the electrical grid power requirements of a cryogenic plant, as well as the size and cost of the plant itself.

[4] The linac convention of $\frac{R}{Q}$ is used here.

[5] This assumes that R_s is uniform over the surface; otherwise, an integral is used.

Accelerators for scientific applications would benefit from cavities with larger peak fields and smaller surface resistances. Achieving H_{pk} close to the predicted H_{sh} of Nb_3Sn would allow high energy linear colliders to reach their design energy with far fewer cavities, potentially reducing costs by billions of dollars for proposed machines [24]. Cavities that reach R_s close to the predicted R_{BCS} for Nb_3Sn would greatly reduce cryogenic plant costs for high duty factor accelerators, such as large circular e^+e^- colliders, light sources, neutron sources, and accelerators for nuclear studies. This could also increase the cost-optimum accelerating gradient, reducing the overall length.

In addition to higher efficiency, there are important operational advantages [25] for working close to atmospheric pressure at 4.5 K instead of at ~2 K.

- Increased reliability of the cryogenic plant, since cold compressors are not used.
- Reduced risk of air leaks causing contamination of the helium (no subatmospheric volumes).
- Relatively easy and fast capacity adjustment to load changes; good turn-down capability.
- Less expensive infrastructure (no 2 K cold box, no cold compressors).
- No superfluid leaks.

In addition to these advantages for large cryogenic plants, higher temperature operation also opens the possibility of cooling a cavity with a cryocooler. While cryogenic plants are highly efficient, they require a great deal of maintenance and operator attention. For small scale industrial accelerators, cryocoolers could greatly reduce infrastructure costs, footprint, and upkeep. Small, high power industrial accelerators would be useful in a wide array of applications, including extreme UV lithography for the semiconductor industry, medical isotope production, border security, and treatment of flue gas and wastewater.

In this paper, we overview the progress towards realizing these advantages of Nb_3Sn as an SRF material and discuss the prospects of current efforts to produce Nb_3Sn cavities. In section 2, we review the properties of Nb_3Sn, and we present a comparative analysis of coating procedures used by several groups. In section 3, we overview measurements on cavities, including CW, pulsed, and other RF results. In section 4, we overview measurements of the microstructure of Nb_3Sn films produced in SRF coating chambers. In section 5, we consider a number of ways that Nb_3Sn cavities in applications may differ from experience with niobium cavities. Finally, in section 6, we conclude with a summary of outlook for Nb_3Sn SRF cavity development.

2. Properties/fabricating Nb_3Sn

2.1. Material properties of Nb_3Sn

Nb_3Sn is an intermetallic alloy in the A15 phase, with a stoichiometric ratio of three niobium atoms to every tin. The stoichiometric crystal structure is shown in figure 2, with the

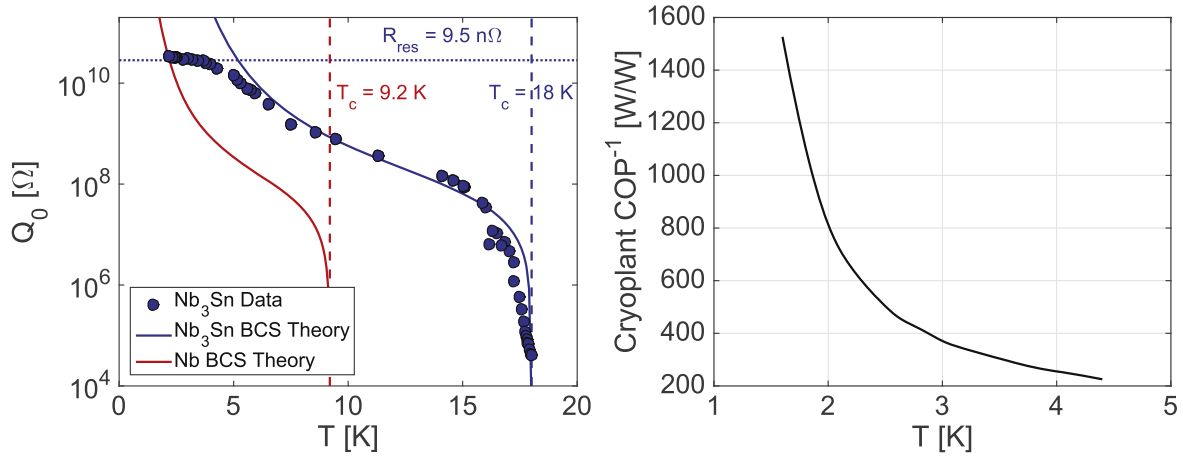

Figure 1. Left: R_s versus T at 1.3 GHz from calculations based on BCS theory for Nb_3Sn and Nb compared to measurement of a Nb_3Sn cavity. Nb_3Sn, with nearly double the T_c of Nb (indicated with dashed lines), offers far smaller R_{BCS} at a given temperature and allows low R_s operation at relatively high temperatures. Right: typical cryogenic plant efficiency given as inverse coefficient of performance (COP^{-1} indicates how many watts of wall power are required to remove one watt of heat) as a function of temperature. Data accounts for Carnot efficiency and deviation of a realistic plant from Carnot [23]. Cryogenic plants operating at ∼4.5 K have substantially higher cryogenic efficiency than those at ∼2 K.

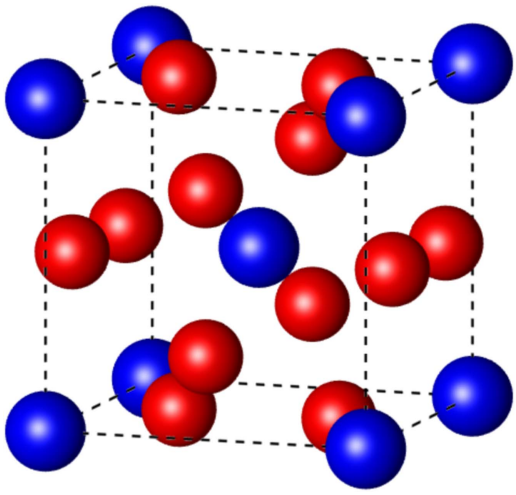

Figure 2. The unit cell of A15 Nb_3Sn, showing the tin atoms in blue and the niobium atoms in red.

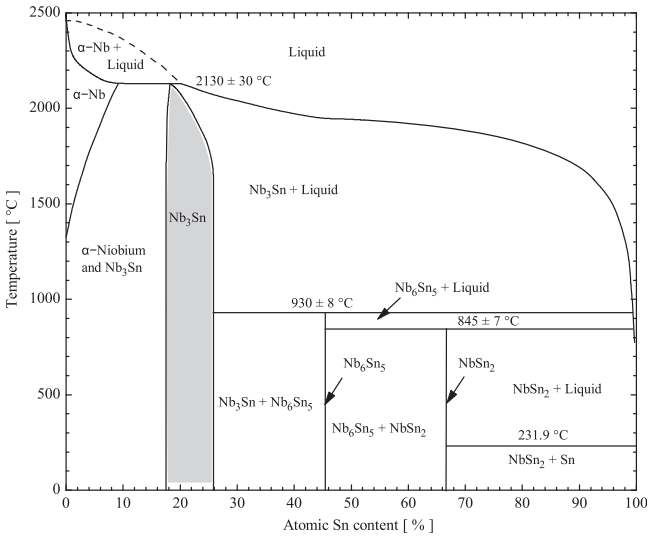

Figure 3. The phase diagram of the niobium–tin system, as measured by Charlesworth *et al* in 1970 (adapted from [29]). The Nb_3Sn-only region has been highlighted.

elements marked. Mechanically, Nb_3Sn is brittle, and a poor thermal conductor. Deformation of a niobium surface that had been coated with Nb_3Sn resulted in extensive fracturing of the coated layer [26], and measurements of the thermal conductivity of Nb_3Sn [27, 28] at 4.2 K is approximately 10^3 times lower than that of niobium. From an engineering standpoint, these properties result in the optimal solution for SRF cavities being a thin film coating of Nb_3Sn on some other, more thermally conductive substrate, such as niobium or copper.

Nb_3Sn has been well known to the superconducting magnet community for some time, and much work has already been undertaken to understand its fundamental properties. A more general review on the material properties of Nb_3Sn was published by Godeke [29]. In this section we will briefly review properties of Nb_3Sn that are most relevant to its use as a superconductor in SRF cavities.

Of primary interest when fabricating Nb_3Sn is the stoichiometry of the material produced. It has been seen, in phase diagrams published by Charlesworth [30] and more recently Feschotte and Okamoto [31, 32], that in the binary system of niobium and tin, the phase Nb_3Sn exists in pure form (without cohabitation with niobium, liquid tin, or other phases of Nb–Sn) for atomic percentages of tin between 17 and 26 percent at temperatures between 950 °C and 2000 °C. This region of solitary existence of the A15 phase is highlighted in the phase diagram shown in figure 3. It is this region of the phase diagram that is of interest for the fabrication of an SRF surface. Extreme tin deficiency will result in areas of uncovered

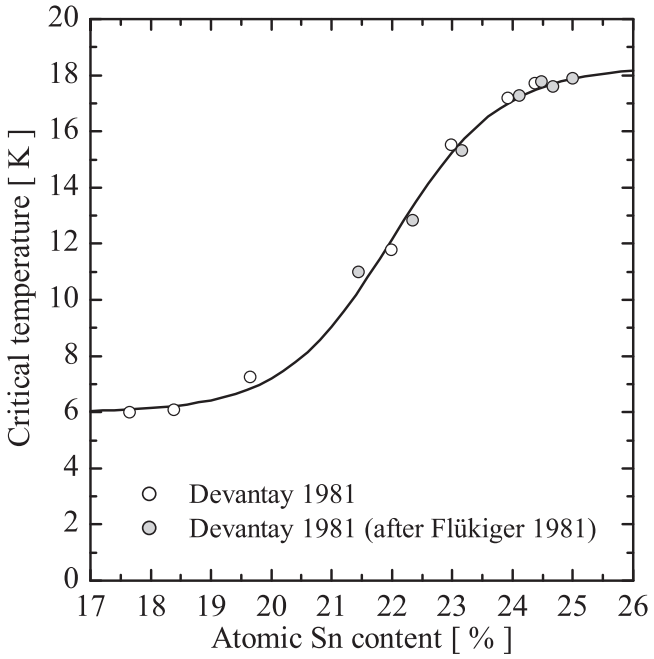

Figure 4. A plot of the critical temperature of Nb_3Sn as a function of the atomic percent tin content, fitted to a Boltzmann function. This plot has been adapted from [29].

niobium; excess tin will result in unreacted tin at high temperatures, or other phases of Nb–Sn at lower temperatures. These low-T_c tin-rich phases are expected to have a far higher RF surface resistance than niobium.

It is not sufficient, however, that the material produced lie in the range of 17–26 atomic percent tin, as the superconducting properties of Nb_3Sn are a function of the atomic percent tin content. Crucially, the transition temperature T_c decreases significantly for atomic percentages of less than 23 percent tin. A plot showing the dependence of this transition temperature on the atomic percent tin, originally published in [29], is shown in figure 4. From this, it can be surmised that, for best performance, the region of the phase diagram that must be achieved lies between 23 and 26 atomic percent tin.

2.2. History of Nb_3Sn in the field of SRF

Nb_3Sn was first shown to demonstrate superconductivity in 1954 [33]. The use of superconductivity for RF cavities was first proposed in 1961, and demonstrated in 1964, with the acceleration of electrons in a lead cavity at Stanford University [34]. The first known attempt at adapting Nb_3Sn for use in superconducting cavities began at Siemens AG in Erlangen, Germany, during the 1970s [35]. They utilized the vapor diffusion method of Saur and Wurm [36] to produce high frequency TE and TM mode cavities. Of particular note is the performance of their X-band TE-mode cavities, whose peak achievable surface RF magnetic fields are still amongst the highest seen to date.

Research into Nb_3Sn for the purposes of SRF was also undertaken around the same time at Kernforschungszentrum Karlsruhe, where studies were performed on the growth process and on the frequency dependence of the surface resistance, as well as at the University of Wuppertal [37]. Work at Wuppertal, which included collaboration with Thomas Jefferson National Laboratory [38], resulted in the production of the first multi-cell cavities coated with Nb_3Sn [39], as well as a number of single-cell 1.5 GHz cavities. Studies on Nb_3Sn SRF cavities during the 1970s through to the 1990s were also performed at CERN [40], SLAC [41], and Cornell [42].

A trend observed in the cavities produced during this time was the presence of a strong Q-slope at surface RF fields exceeding 30–40 mT [38, 43]. Although the quality factor at low fields exceeded that of niobium cavities of the period [44], the reduction in efficiency at higher gradients impaired the feasibility of using the material as an alternative to niobium. Due to the onset of the Q-slope at fields corresponding to the lower critical field of Nb_3Sn, it was thought that the slope was due to magnetic flux entry into the material [38] resulting in increased losses.

The research programs at Siemens AG, Karlsruhe, and Wuppertal had shut down by 2000. Development of Nb_3Sn SRF coatings via the vapor diffusion technique was resumed several years later when, in 2009, a research program began at Cornell University that produced cavities using an adaption of the Wuppertal method [45]. The 1.3 GHz single-cell cavities produced by this program did not show the same onset of Q-slope seen previously, maintaining high quality factors in excess of the lower critical field and demonstrating that the slope was not a limitation fundamental to Nb_3Sn. At the turn of the decade a program was started at Jefferson Lab, which uses an adaptation of the Siemens method [46] to coat 1-cell, 2-cell, and 5-cell 1.5 GHz cavities. More recently, a program was initiated at Fermi National Accelerator Laboratory [47], again using a method similar to Wuppertal, with the intent of coating even larger structures such as 9-cell 1.3 GHz cavities. At the time of writing, the programs at Cornell, Jefferson Lab, and Fermilab continue active research and development of Nb_3Sn cavities.

Programs to produce Nb_3Sn coatings by methods other than vapor diffusion have also made continuing progress throughout the current decade, such as chemical vapor deposition, liquid tin dipping, multilayer sputtering, mechanical plating, electron beam coevaporation, bronze processing, and electrodeposition (many of these are followed by an annealing step at high temperature) [48–58]. Advantages of these procedures can include reduction in material costs (e.g. through the use of copper substrates) or reductions in the reaction temperature. Possible disadvantages are contamination of the RF layer with residual copper, formation of undesirable phases, non-uniform coatings, very high surface roughness, and very small grain sizes (which have been linked to weak link grain boundary effects [59]). To date, these methods have not produced cavities whose performance exceeds that of those produced using vapor diffusion, a comparatively more developed method that will be the focus of this paper.

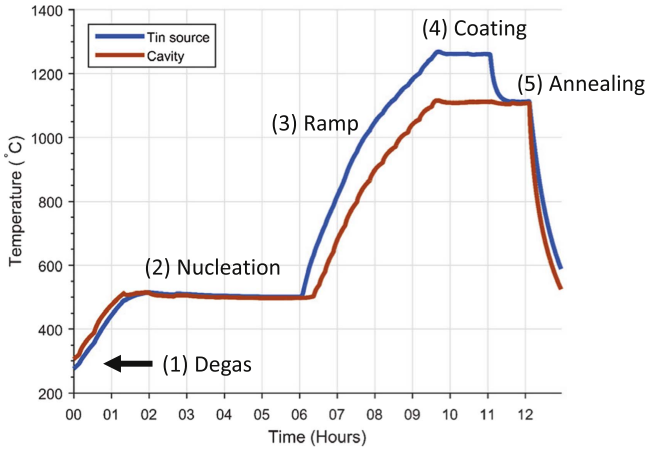

Figure 5. Temperature profile of the coating furnace used at Cornell University since February 2016. The temperature of the cavity and the tin source are given separately, reflecting the presence of the second hot zone. The steps indicated on the temperature profile are explained in the text.

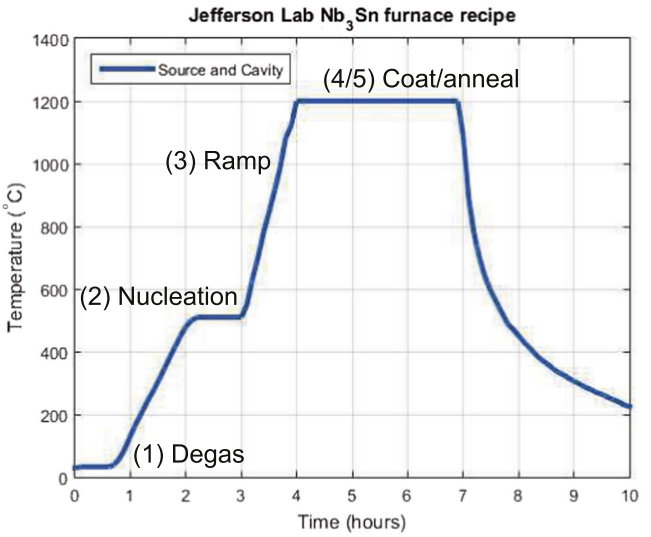

Figure 6. An example of the coating recipe used at Jefferson Lab [46]. The five different elements of a coating, described in the text, have been identified on the chart.

2.3. Fabrication of Nb_3Sn using vapor diffusion

All coatings made using the vapor diffusion process possess similar features in their coating temperature profiles, and equivalent steps can be identified. An example coating profile used at Cornell University, shown in figure 5, demonstrates all the steps utilized to date:

(i) A degas stage. The chamber is taken to a temperature between 100 °C and 200 °C and parked at this temperature. During this time, active pumping on the chamber removes residual moisture, etc, that may have been introduced during the opening of the furnace and the placing of the part.

(ii) A nucleation stage. At this stage, the chamber is taken to an intermediate temperature, during which time nucleation sites are created on the surface of the substrate. Historically, this has been done either by pre-anodization and the introduction of a temperature gradient during the ramp-up (Siemens) [60], or the use of a nucleation agent such as SnF_2 (Siemens) or $SnCl_2$ (Siemens, Wuppertal, Cornell, Jefferson Lab) [26]. Using a nucleation agent instead of pre-anodization helps to prevent uncovered areas, but avoids the RRR degradation that has been observed after growing a thick oxide and then diffusing it into the bulk of the niobium substrate [44, 61].

(iii) A ramp to coating temperature. Beginning from the intermediate temperature of the nucleation stage, the secondary heating element is often activated at this stage, if it is present. The chamber is then increased to the desired coating temperature.

(iv) The coating stage. The cavity is held at a constant temperature above 950 °C, at which temperature the low-T_c phases of Nb–Sn (Nb_6Sn_5 and $NbSn_2$) are thermodynamically unfavorable. During this phase, the layer grows on the surface of the niobium, as tin consumed in the production of the layer is replenished by the tin source. During this stage, the tin source is held at a temperature higher than the part, in the event that a secondary heating element around the tin source is present.

(v) An annealing stage. In the event that a secondary heater is not present, this stage is likely to be identical to the coating stage. If a secondary heater is present, then it is closed and/or turned off and allowed to cool, thus reducing the rate of tin arriving at the surface of the part. During this time, the chamber is held at a temperature above 950 °C, often at the same temperature at which it was held during the coating stage. The purpose of this step is to allow any excess of pure tin at the surface of the part to diffuse into the layer and form Nb_3Sn.

Virtually all temperature profiles published to date can be described using a succession of these five stages, although the first two steps—degas and nucleation—are sometimes omitted. Furthermore, in the absence of a secondary heater, the coating and annealing stage are often indistinguishable from one another based on the temperature profile alone. An example coating profile from Jefferson Lab is shown in figure 6, identifying the stages used.

During the coating stage, in which tin is being transferred, it is critical that the temperature of the tin gas is sufficiently high enough to ensure a uniform coating. A high temperature tin gas possesses an elevated vapor pressure and consequently, a short mean free path. When coating complex structures such as SRF cavities, in which the tin gas must diffuse about the structure in order to coat surfaces that do not have direct line of sight on the tin source, the mean free path should be less than the characteristic length scale of the cavity.

In figure 7, the vapor pressure for tin and tin(II) chloride is shown as a function of temperature. The mean free path, l, is then calculated using the relation [64]

$$l = \frac{k_b T}{\sqrt{(2)}\pi d^2 p}, \tag{4}$$

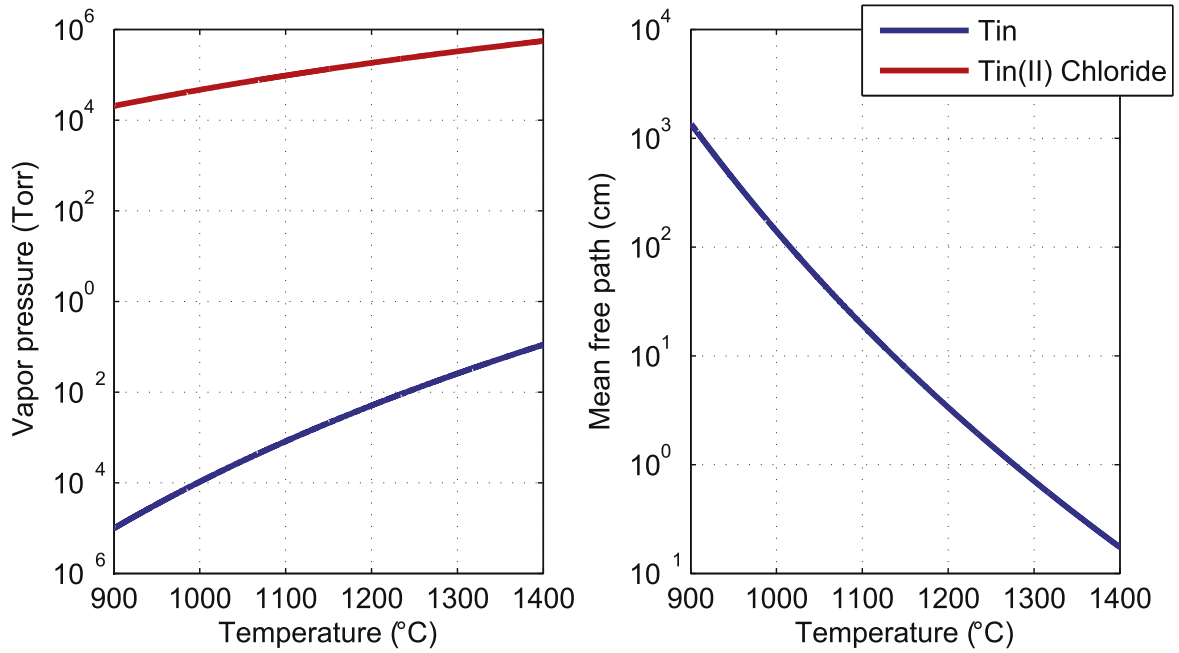

Figure 7. The vapor pressure (left) of tin(II) chloride and tin as a function of temperature, with tin data from [62] and tin(II) chloride data from [63]. The corresponding mean free path (right) for tin is also shown as a function of temperature.

where T is the temperature of the gas, d the van der Waals diameter of the atom (450 pm in the case of tin), and p the vapor pressure of the gas. The mean free path as a function of the gas temperature in Celsius is also shown in figure 7. From this we can surmise that when coating a 1.3 GHz single-cell cavity, with an iris diameter of approximately 7 cm, a tin gas temperature of 1200 °C or greater is necessary to ensure a uniform coating.

From the vapor pressure it is also possible to calculate the evaporation rate of the tin source. This is useful to know, as it gives both a first order estimate of the rate of tin arrival at the cavity surface, as well as the amount of tin left in the source at any point during the run if the initial amount was known. The evaporation rate of the tin source can be obtained using the Langmuir formula for evaporation, such that [65]

$$\frac{\mathrm{d}M}{\mathrm{d}t} = Ap\sqrt{\frac{m}{2\pi k_{\mathrm{b}} T}}, \tag{5}$$

where M is the mass of tin in the crucible, A is the area of the mouth of the tin source, and m is the mass of a tin molecule. By integrating this evaporation rate with respect to time over the temperature profile of the tin source, and with knowledge of the initial amount of tin placed into the furnace, the final amount of tin remaining can be calculated, and cross-check with measurements done post-coating. Use of this method for monitoring coating procedures at Cornell has found that the calculated and measured values of tin remaining agree to within ±5% [66].

2.4. Comparison of coating processes used at different institutions

The original design utilized by Siemens consisted of a quartz ampulla, serving as a reaction chamber, inside which a crucible bearing tin was placed alongside the niobium piece to be coated. However, initial results quickly demonstrated that at the temperatures involved, contamination from the quartz was affecting the Nb_3Sn produced [67]. Therefore, the coating design was altered such that the interior of the niobium cavity to be coated became the reaction chamber, thus avoiding unwanted contamination.

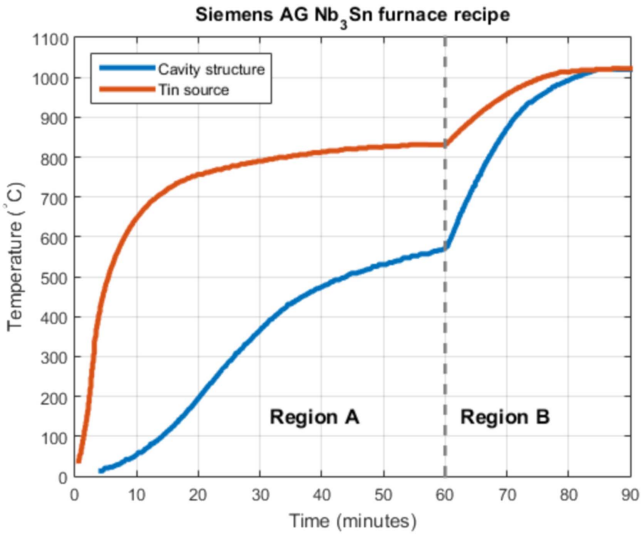

Figure 8. Temperature profile used by Siemens when utilizing a temperature gradient [68]. First, the ampulla containing the tin source and the cavity is only partially inserted into the furnace hot zone, resulting in a temperature gradient (region A). Once the gradient has been sufficiently established, the ampulla is fully inserted into the hot zone and allowed to come to coating temperature (region B).

In early coatings performed at Siemens, it was found that the Nb_3Sn layer showed significant non-uniformity—large

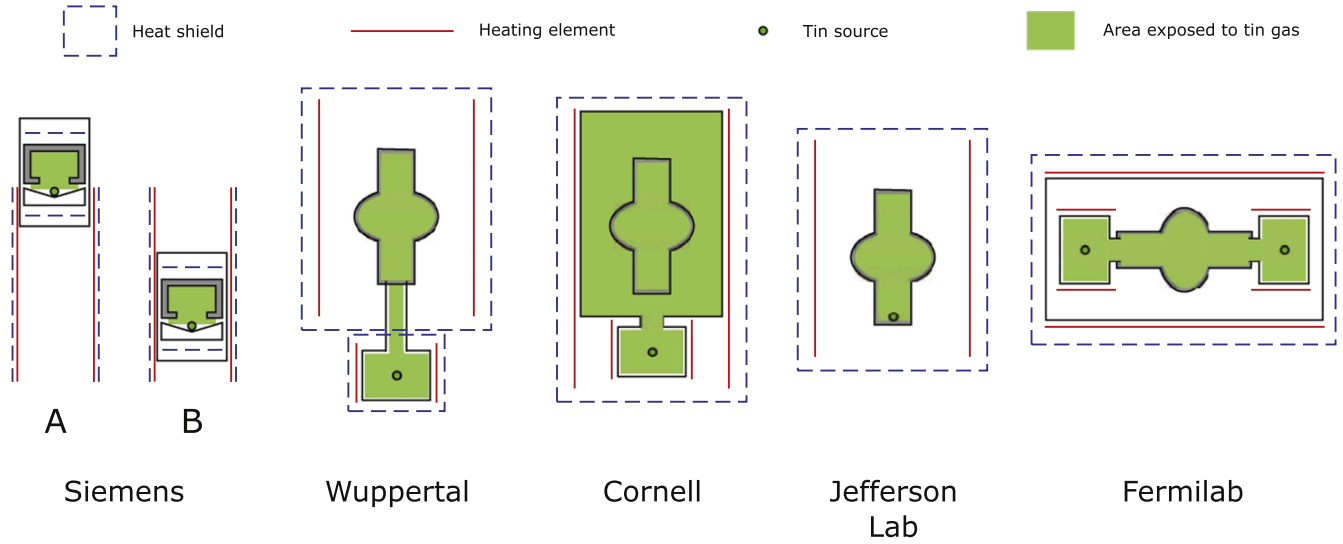

Figure 9. Simplified schematics for the different coating furnaces highlighted in this paper, namely those of Siemens AG, the University of Wuppertal, Cornell University, Jefferson Laboratory, and Fermi National Laboratory. In the Siemens furnace, two configurations (A and B) are used during a coating, the first corresponding to the region of temperature gradient seen in figure 8, and the second to the coating step of figure 8.

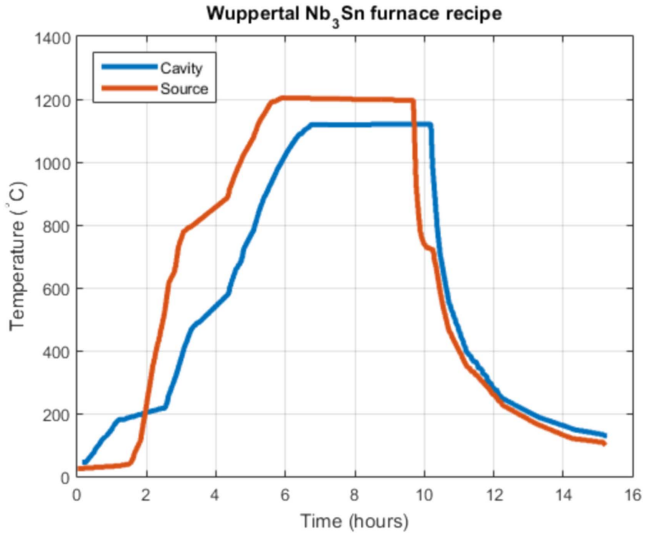

Figure 10. An example of the coating recipe used at Wuppertal. In contrast to the Siemens recipe used previously, the Wuppertal recipe is distinguished by the use of a secondary hot zone surrounding the tin source.

regions of Nb would remain essentially uncoated [26]. The suspicion was that uneven nucleation of the surface was resulting in a non-uniform surface; this issue was resolved through the use of (separately or in tandem): (1) a temperature gradient between the tin source and the cavity during the initial temperature ramp, as in figure 8 [68], (2) growing the oxide layer of the Nb part through electrolytic anodization, and (3) the use of a nucleation agent such as $SnCl_2$ or SnF_2. Thanks to these changes to the coating method, the TM and TE cavities whose results are shown later in this paper were produced.

The coating method used later, at the University of Wuppertal, made an important change to the process: the addition of a second heating zone, surrounding the tin crucible [69]. This allowed for separate temperature control of the niobium part to be coated and the tin source. In coatings of cavities done at Wuppertal, the tin source was held at a higher temperature than the cavity, as seen in the temperature profile shown in figure 10. To avoid the issues of surface non-uniformity seen in early Siemens coatings, $SnCl_2$ was introduced into the furnace alongside the tin, to ensure uniform nucleation. Schematics comparing the furnace setups of Siemens and Wuppertal can be seen in figure 9.

The furnace designs of both Siemens and Wuppertal have been replicated, as least in part, at Jefferson Laboratory and at Cornell University, respectively . The Cornell design incorporates a second heating element around the tin source, allowing the tin source to be held at a higher temperature than the part to be coated. The furnace design at Jefferson Lab does not incorporate a second hot-zone, with the tin source and substrate being always held at the same temperature. A Nb_3Sn coating apparatus at Fermi National Accelerator Laboratory, under construction at the time of writing, includes two separate sources, mounted at either end of the cavity, thus allowing for an even coating of larger structures such as 9-cell 1.3 GHz cavities. Simplified diagrams of the furnaces used at Cornell, Jefferson Lab and Fermilab are also shown in figure 9.

3. Cavity results

3.1. CW measurements

A diverse range of cavity geometries have been coated with Nb_3Sn and tested. In this section, we overview CW measurements, with a focus on the results with the highest fields.

Though their geometry is not generally applicable to acceleration, the 10 GHz TE cavities coated by Siemens had the highest maximum peak magnetic fields reported in the

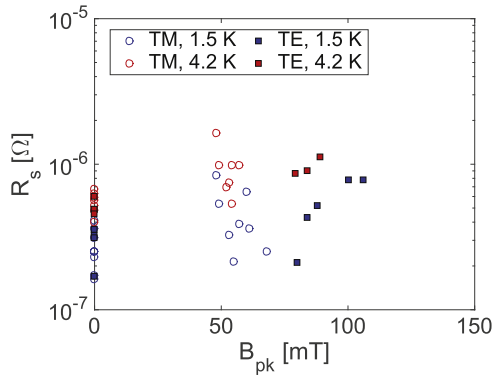

Figure 11. 1.5 and 4.2 K measurements of some of the highest performing Nb_3Sn TM and TE 10 GHz cavities produced by Siemens. Data from [26, 70], which report Q_0 at zero field and at the maximum field.

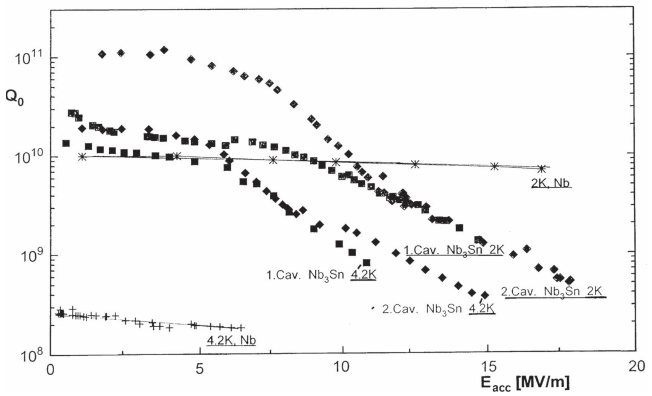

Figure 12. 2.0 and 4.2 K Q_0 versus E_{acc} measurements of some of the highest performing Nb_3Sn 1.5 GHz single cell cavities produced by U. Wuppertal. Data from a niobium cavity is shown for comparison. Figure adapated from [43].

literature. As shown in figure 11, the maximum fields were as high as 106 mT, about 30% higher than those achieved in CW mode in cavity types more commonly used in accelerators. The results show that even with $R_s \approx 1\ \mu\Omega$, such fields can be sustained on Nb_3Sn surfaces without thermal instability. Siemens produced more than 50 coatings of TE cavities, and they showed that the maximum fields were normally distributed, suggesting that random defects were the cause for limitation [70]. Siemens also produced a smaller number of coatings on TM cavities (some results from TM cavities are also shown in figure fig:siemens), but the maximum fields of these cavities were smaller, as high as 84 mT [70], possibly due to geometrical differences or simply to limited statistics. For both the TE and the TM cavities, the surface resistance values were close to the BCS predication at 10 GHz.

Siemens researchers studied a variety of coating parameters and post-treatment processing. They showed that they could achieve far higher maximum fields and quality factors when active pumping was employed, rather than sealing off the reaction chamber before inserting the chamber to the furnace[6]. Small changes were also observed by oxypolishing to remove a small amount of material (pitting and degradation occurred above 200 V).

At University of Wuppertal, cavities were coated that had shapes and frequencies used in accelerators. Researchers made the critical observation that the Q_0 of these cavities is strongly influenced by the cooldown. A slow, uniform cooldown produces higher Q_0, which was traced to thermocurrents between the niobium and Nb_3Sn layers [71]. Wuppertal researchers also observed a strong increase in heating after quench, localized in the quench location, which they also attributed to thermocurrents as the area cooled down again below T_c.

Two of these Wuppertal cavities were elliptical single cell 1.5 GHz cavities with the CEBAF shape [72, 73] that were tested at Jefferson Lab, as shown in figure 12 [43]. The maximum gradient for these two cavities was promising, with E_{acc} as high as 18 MV m^{-1}. Furthermore, the Q_0 at low fields was 2×10^{10} at 4.2 K, and 10^{11} at 2.0 K, several times higher than could be achieved with Nb at these temperatures. However, both cavities were afflicted with strong Q-slope, a reduction of the quality factor with increasing E_{acc}, such that at the highest fields, the Q_0 was below 10^9. Neither cavity quenched—the limitation was the available RF power. Temperature mapping studies were also carried out at Jefferson Lab, showing broad areas of heating in the Q-slope region. Noting the reproducibility of these results, researchers questioned if the degradation may be caused by a fundamental loss mechanism that occurs above the expected H_{c1} of Nb_3Sn [38, 74], since the onset of the Q-slope at $E_{acc} \sim 5$ MV m^{-1} corresponds to when the peak magnetic field is approximately equal to H_{c1} of Nb_3Sn [75, 76]. One explanation for why this might occur would be if surface disorder compromised the energy barrier that prevents flux expulsion above H_{c1}, when the superconductor is in the metastable state. The coherence length ξ indicates the size of surface disorder that a superconductor is sensitive to, and in Nb_3Sn ξ is expected to be 3–4nm [75] much smaller than that of processed niobium ~23 nm[7], making it more vulnerable. If in fact this behavior were fundamental, and Nb_3Sn were limited to high R_s above 5 MV m^{-1} [38, 74], it would be far less useful in SRF accelerators.

Whether surface resistance of order 10 nΩ could be maintained to medium fields remained an open question for over a decade, when new results were reported from Cornell. The first single cell 1.3 GHz cavity that was coated and tested at Cornell had strong Q-slope (similar to U. Wuppertal cavities) and high residual resistance that was traced to one of the half cells through temperature-mapping studies (see figure 13) [79]. However, cavities that were coated and tested later exhibited 4.2 K Q_0 of $\sim 2 \times 10^{10}$ at low fields, and they reached medium fields without the strong Q-slope that had been observed previously. These cavities consistently reached quench fields of 14 MV m^{-1} or higher, with $Q_0 \sim 1 \times 10^{10}$ at 4.2 K, showing proof of principle that Nb_3Sn could outperform Nb at gradients and frequencies that are useful in

[6] Data from figure 11 are from cavities coated with active pumping.

[7] This value was obtained assuming RRR = 10 and using equations from [77] and clean values from [78].

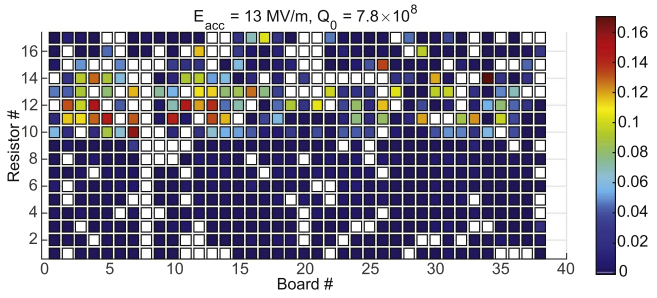

Figure 13. Temperature map of the first 1.3 GHz single cell cavity coated at Cornell. The plot shows heating over the surface of the cavity measured by an array of temperature sensors measuring parallel to the cavity axis (parallel coordinate given by Resistor #) and azimuthally around the cavity (azimuthal coordinate given by Board #). The strong heating in half the map indicates that one half-cell had significantly higher losses than the other. Figure from [79].

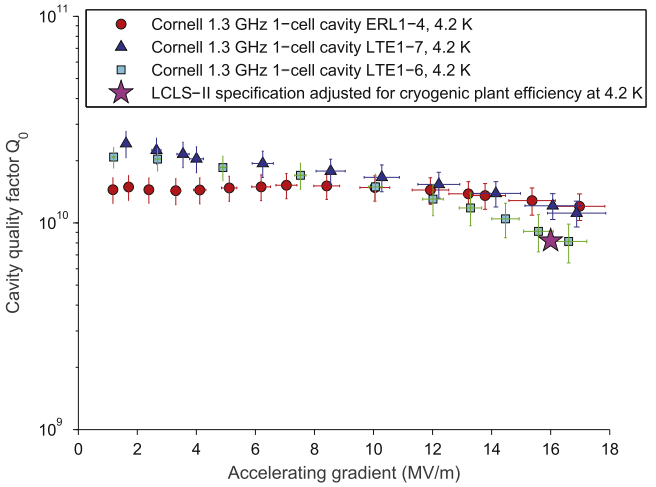

Figure 14. Quality factor versus accelerating gradient curves taken at 4.2 K for the three 1.3 GHz single-cell cavities in use as of February 2016 in the Cornell Nb_3Sn program. Shown for comparison is the Q_0 specification for LCLS-II, adjusted for the increased efficiency of operating at 4.2 K. Figure from [80].

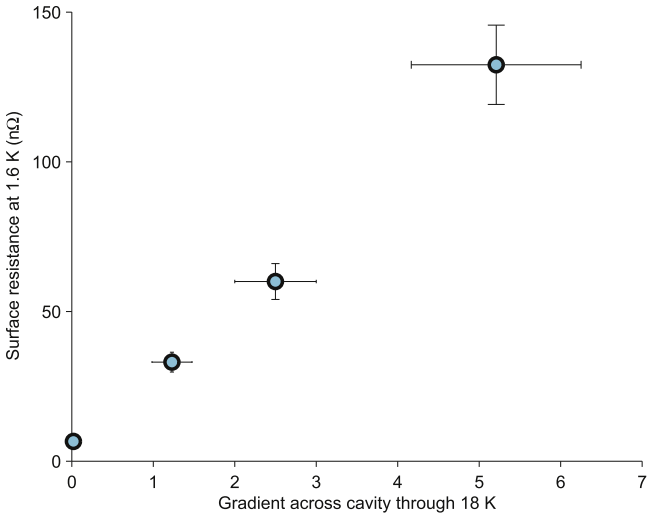

Figure 15. The surface resistance measured at 1.6 K and 5 MV m^{-1} for a 1.3 GHz single-cell cavity cooled in different thermal gradients, as measured from iris-to-iris. Figure from [80].

applications. 4.2 K Q_0 versus E_{acc} curves from several Cornell cavities are plotted in figure 14. To make a useful comparison to a state-of-the-art high Q_0 SRF accelerator, the specification for E_{acc} and Q_0 for cavities in LCLS-II was plotted in this graph, after multiplying by a factor of 3.3 to account for the approximate difference in cryogenic efficiency between a cryogenic plant operating at 4.2 K compared to 2 K (see figure 1).

The absence of strong Q-slope in these cavities may be related to a reduction in the quantity of low tin content material in the RF layer (see section 4). Additional experiments, especially with coupons cut from cavities after RF test, can help to develop understanding of how microstructure effects strong Q-slope. Another factor that has a smaller but still significant impact on Q-slope is the temperature uniformity during cooldown, as shown in figure 15. Experiments at Cornell show that even a ~40 mK difference in temperature uniformity during cooldown can change the 4.2 R_s at maximum fields by a factor of ~2 [81].

Measurements of R_s versus T and f versus T were fit using the SRIMP program [82–85] that was developed to use computations based on BCS theory to correlate to material parameters. The extracted material parameters were used to determine the critical fields for the cavities that were coated at Cornell. The results, some of which are presented in figure 16, show that taking into account uncertainty in measurement and fitting, the cavities reproducibly exceeded H_{c1} without the strong Q-slope that had been observed in Wuppertal cavities.

At Jefferson Lab, Nb_3Sn cavities were produced and tested that show Q-slope similar to U. Wuppertal, as shown in figure 17. Researchers hypothesize that the Q-slope may be due to contamination from Cl (from $SnCl_2$) or Ti (from NbTi flanges), or it may be due to variation in the coating composition [46].

3.2. Pulsed measurements

CW measurements are helpful to predict cavity performance in an accelerator, but they can be limited by small defects. A small defect can cause overheating above the critical temperature, creating a spreading area of normal conducting material that quenches the cavity on millisecond timescales. To reduce the effect of small defects, cavities can be tested with short pulses of high power RF, to fill the cavity with energy and cause quench on tens of microsecond timescales.

Pulsed measurements on Nb_3Sn cavities have been performed by Campisi at SLAC in the 1980s [86], Hays at Cornell in the 1990s [87], and Posen and Hall at Cornell in the 2010s [81, 88]. Measurements are plotted in figure 18. The general trend is similar: close to T_c, the data agree with the superheating field, H_{sh} of Nb_3Sn, and at lower temperatures, the data diverge towards lower fields. The trend is consistent with defect behavior, suggesting that the low temperature behavior is not fundamental and if the defect behavior could be eliminated, the maximum field would extrapolate close to $\mu_0 H_{sh} \sim 0.4$ T [88].

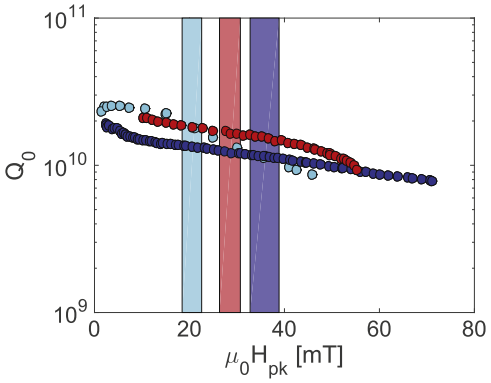

Figure 16. 4.2 K Q_0 versus $\mu_0 H_{pk}$ measurements of three different coatings of Nb_3Sn 1.3 GHz single cell cavities produced at Cornell. For each curve, a shaded area of a corresponding color shows the extracted H_{c1} values with uncertainty. No degradation is observed when the peak field reaches H_{c1} for any of these coatings. Figure adapted from [79].

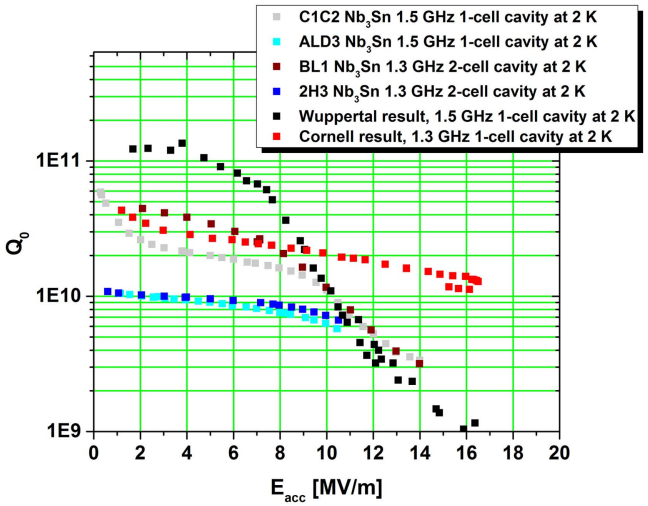

Figure 17. Recent measurements of Nb_3Sn cavities coated and tested at Jefferson Lab, compared to Wuppertal and Cornell. Q-slope similar to Wuppertal is observed. Figure adapated from [46].

Applying square pulses from the RF source with different forward power levels, the quench field was also measured as a function of time to quench. If a fundamental field limit were being reached, the quench field should be independent of the forward power. However, measurements presented in figure 19 show a different trend. As the forward power is increased, the quench field increases as well. Heating at defects could account for this trend: if the cavity fills with RF energy faster, higher fields can be reached before defect heating has time to cause quench.

3.3. Other RF measurements

Karlsruhe researchers measured R_{res} as a function of frequency using different modes of Nb_3Sn-coated helical resonators and cylindrical cavities [89]. They observed an approximate f^2 dependence of the residual resistance, which is predicted in models of losses at grain boundaries [8, 90].

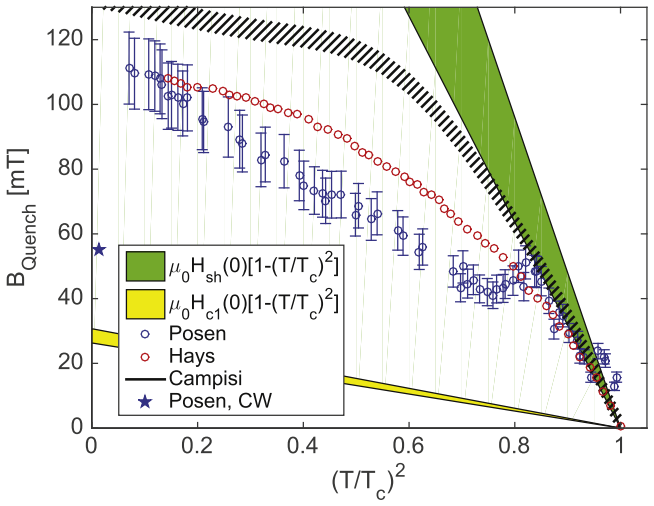

Figure 18. Pulsed quench field as a function of temperature for measurements from Campisi, Hays, and Posen [86–88]. Results from CW measurements are also plotted for the data from [88]: quench field, H_{c1}, and H_{sh}.

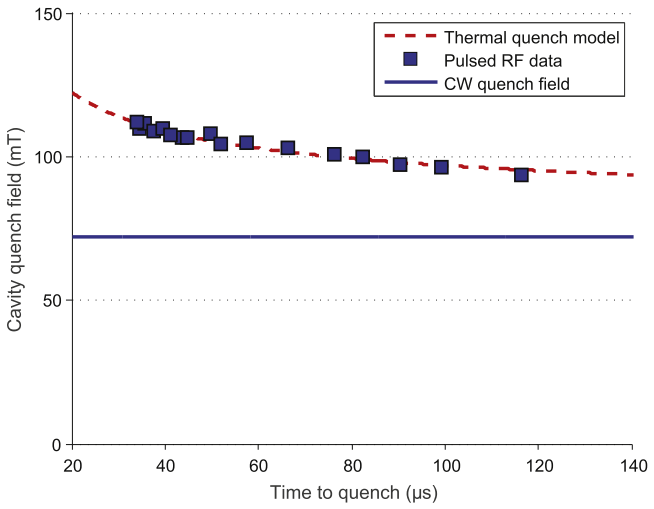

Figure 19. Plot of the peak field achieved in a 1.3 GHz single-cell cavity as a function of the time taken to achieve this field during high-pulsed-power RF testing. As the input power is increased, the time to quench is reduced. As the fill time of the cavity decreases, thermal limitations are slowly overcome. Figure from [80].

University of Wuppertal researchers also suspected that grain boundary losses can have a substantial impact on performance in their RF measurements [91]. They observed strongly nonlinear heating in films that increased in severity as they grew films with smaller grain sizes. Their analysis implicated weak links between grains as the cause for this nonlinearity.

Of particular concern in the operation of a superconducting cavity is the impact of external DC magnetic fields upon the performance of the cavity. Superconducting cavities, particularly when cooled slowly (as must be done for a Nb_3Sn cavity), will trap a percentage of the externally applied magnetic field. This trapped flux will result in an increase in the residual resistance of the cavity proportional to the amount of flux trapped, and thus an increase in the surface

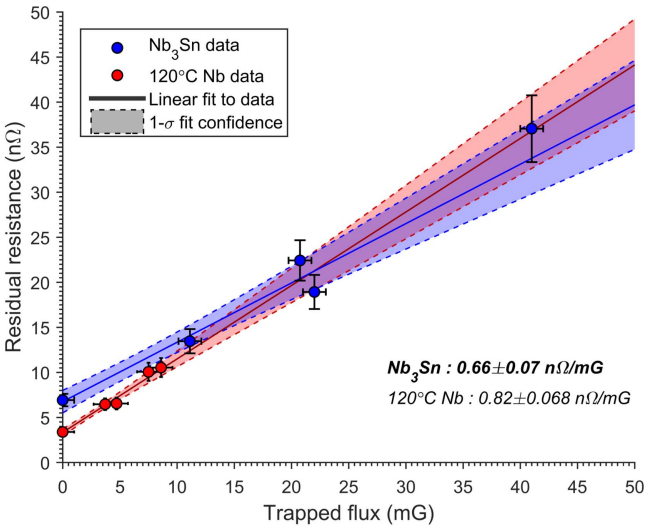

Figure 20. The residual resistance of a 1.3 GHz single cell cavity coated with Nb_3Sn at Cornell, measured at 1.6 K and 5 MV m^{-1}—and, for comparison, a more conventional 120°C-baked Nb cavity of the same shape—as a function of the ambient field trapped in the cavity walls during cooldown. Figure from [80].

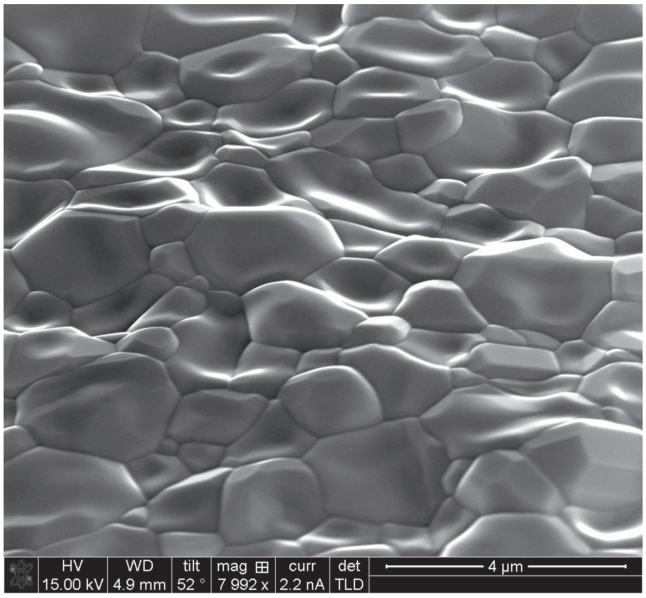

Figure 21. An SEM image (taken at an angle) of the surface of a coupon coated with Nb_3Sn at Cornell. The surface shows features similar to those produced by other labs using the evaporation–deposition method. Image from [79].

losses with correlated drop in cavity efficiency. The constant of proportionality relating the amount of flux trapped to the increase in the residual resistance will be referred to as the sensitivity to trapped flux, and will be quoted in nΩ of residual resistance gained per mG of field trapped.

By deliberately applying an external magnetic field during a cavity test, the sensitivity can be measured. Remarkably, Nb_3Sn was found to be no more sensitive to trapped flux than bulk niobium that has received a 120 °C bake following standard bulk chemistry. This is demonstrated in figure 20. Experimenters have shown that with bulk niobium cavities, it

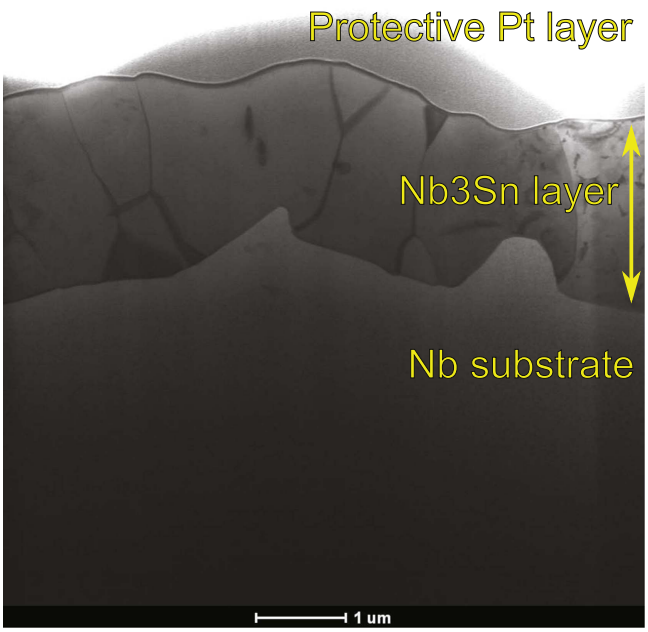

Figure 22. A STEM bright-field image taken at 120 kV of a cross-section of a Nb_3Sn-on-Nb prepared using focussed ion beam (FIB) lift-out techniques. The Nb_3Sn layer, protected from the FIB by a protective platinum layer, demonstrates a roughly columnar grain structure and a distinct boundary with the niobium substrate.

is possible to expel ambient magnetic flux by cooling with a thermal gradient across the cavity [92]. However, due to the thermal currents generated by the Seebeck effect in Nb_3Sn cavities, such a fast cooldown is not permissible, and therefore a reasonably small sensitivity to trapped flux is important.

4. Microscopic measurements

When grown on niobium, Nb_3Sn forms distinct grains easily distinguishable when viewed using a scanning electron microscope (SEM), as seen in figure 21. Atomic force microscopy measurements carried out at Jefferson Lab [46] and at Cornell [81] on samples produced at the respective labs demonstrate that as-grown Nb_3Sn has a surface roughness on the same order as the grain size, which in most cases is on the order of a micron. A series of measurements performed at Jefferson Lab [46] on substrates receiving different preparations show that substrate preparation has no impact on the roughness. In particular, there appears to be no difference in the roughness of a Nb_3Sn layer coated on niobium substrates that have received a buffered chemical polish (BCP) or an electro-polish (EP), two commonly used chemical etches for the preparation of niobium cavities. This correlates with previous cavity measurements at Cornell, which demonstrated no significant difference in performance between Nb_3Sn cavities whose substrates had been prepared using EP or BCP [79].

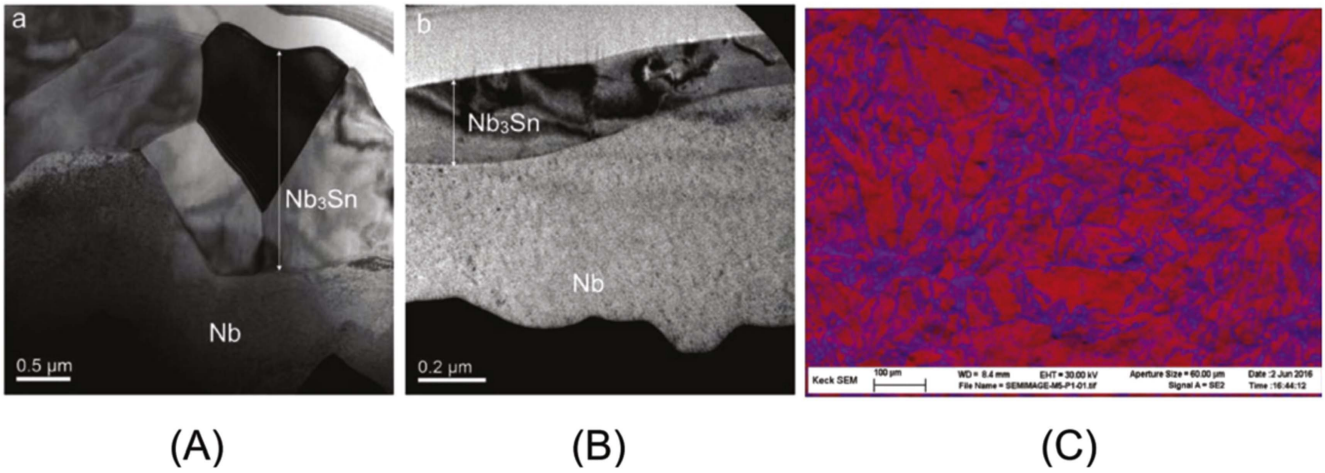

Figure 23. (A) A cross-section of a more commonly seen layer that shows a depth of approximately 3 μm, compared to (B) a cross-section of a thin film region, which is of insufficient thickness to screen the bulk from the RF field. Images from [99]. The extent of these regions can be seen in (C), an EDS map of a cavity cut-out from a region that showed excessive heating during RF testing. In this map, blue regions indicate a thick region, and red a thin region whose thickness is on the order of the RF penetration depth.

Thickness measurements carried out at Wuppertal [93] found, in agreement with previous literature [94, 95], that the thickness of the layer formed at a reaction temperature of 1150 °C follows the relation

$$d_{\text{film}} = d_0(T)t^{0.38}, \tag{6}$$

where d_{film} is the thickness of the film in microns, $d_0(T = 1150\ ^\circ\text{C}) = 1.3\ \mu\text{m}$ for a reaction temperature of 1150 °C, and t is the time in hours. Further measurements also gave an approximate dependence of the prefactor $d_0(T)$ on the reaction temperature for temperatures greater than 1000 °C.

Thickness measurements done using x-ray sputtering (XPS), at Wuppertal [93], Siemens [96], Jefferson Lab [97], and Cornell [79], show a layer of uniform stoichiometry up to a depth of 2–3 μm. This is confirmed by transmission electron microscopy (TEM) of cross-section cutouts performed at Argonne National Laboratory [98], which shows a layer of thickness varying between 2 and 4 μm. An example of such a cross-section, taken from a sample coated at Cornell, is shown in figure 22. The transition from the Nb_3Sn film to the niobium substrate is sharp and distinct. The grain structure is equally distinct, with clear grain boundaries. Many grains display a columnar structure, extending from the RF surface all the way down to the interface with the niobium bulk.

Although XPS measurements indicate a constant stoichiometry within 2–3 μm deep within the layer, TEM-EDS measurements carried out on cross-sections at Argonne show regions within the layer that show a deficiency of tin relative to neighboring regions [98]. Furthermore, some of these regions of tin-depletion have been found a distance on the order of the RF penetration depth from the surface of the layer. Since tin depleted Nb_3Sn has a considerably lower critical temperature, the presence of such a poor superconductor within the realm of influence of the RF field will have a negative impact on the RF performance of the layer due to the increased losses in these tin depleted regions. It is entirely possible that these regions could be the limiting factor in accelerating gradient at this time, as thermal runaway within the layer induced by the presence of these lossy tin depleted phases and the poor thermal conductivity of Nb_3Sn causes the cavity to quench.

Another interesting feature observed in recent studies of samples and cavity cut-outs are regions of exceptionally thin Nb_3Sn coverage [99, 100]. Originally seen in cut-outs from regions of a cavity that showed significant surface heating during RF testing, these regions have since been discovered, to lesser extent, in samples coated using coating procedures that have produced cavities capable of accelerating gradients of 16 MV m^{-1} with Q's of $>10^{10}$ at 4.2 K [101]. These regions have been found to be of a thickness on the order of the RF penetration depth, and are thus insufficiently thick to screen the bulk from the RF field. To illustrate this, a cross-section of both a 'standard', sufficiently thick layer is shown in figure 23(A), which stands in stark comparison to the cross-section of a thin region as seen in figure 23(B), which clearly shows the insufficient thickness of these regions. The extent of these regions seen at some cavity cut-outs, as seen in figure 23(C), and the enhanced heating seen at these regions during RF testing, imply that these regions are responsible for increased surface losses. Studies are ongoing to understand the growth mechanics of these regions and methods for suppressing their formation.

Researchers from Jefferson Lab have performed electron backscatter diffraction studies of Nb_3Sn layers to examine the grain orientation, as shown in figure 24. They found that the grain orientation is independent of the substrate [102]. This is consistent with previous observations that uniform coatings could be achieved regardless of crystal orientation of the substrate if the substrate was anodized or nucleated with tin halides [44, 60].

5. Considerations in applications

RF measurements from section 3.1 are proof of principle that Nb_3Sn cavities can be useful in applications, but there are a

Figure 24. EBSD image of a cross section of a Nb_3Sn coating measured at Jefferson Lab. The measurement suggests that the grain orientation is independent of the substrate. Image from [102].

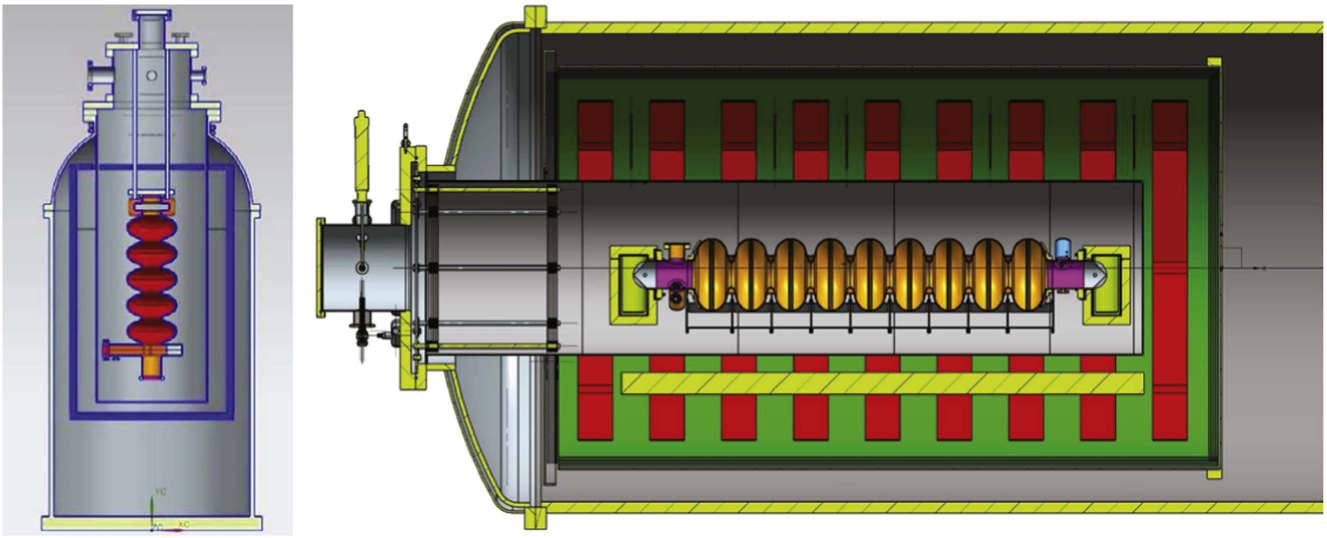

Figure 25. Left: the Nb_3Sn coating apparatus at Jefferson Lab is being modified for coating 1.5 GHz 5-cell cavities with waveguide endgroups [102]. Right: an apparatus is being fabricated at Fermilab for coating 1.3 GHz 9-cell and 650 MHz 5-cell cavities.

number practical considerations that should be carefully evaluated prior to putting Nb_3Sn cavities into an accelerator. Several of these have been resolved favorably. For example, the latest cavities from Cornell showed that the standard cleaning method of high pressure water rinsing can be applied prior to reaching high Q_0 at medium fields. The tests of Siemens cavities and Wuppertal cavities showed remarkable power dissipation without global thermal instability: Siemens cavities reached 106 mT with $R_{res} \sim 1\ \mu\Omega$, and Wuppertal cavities reached 80 mT with $R_{res} \sim 0.5\ \mu\Omega$, giving optimistic prospects for reaching higher fields without global thermal instability in cavities with $R_{res} \sim 10$ nΩ. As described in section 3.3, residual resistance due to trapped external magnetic fields is expected to be close to that of niobium. Similarly, multipacting in Nb_3Sn cavities is not expected to be worse than that in Nb cavities, based on measurements of secondary electron yield [103].

One important practical challenge for Nb_3Sn is scaling up to production-style cavities. Past experience on a 500 MHz single-cell cavity and a 3 GHz 5-cell cavity showed maximum fields of only $\sim$5 MV m^{-1}, with heating observed in temperature maps that experimenters linked to defects (one contributing factor may have been the use of low RRR niobium in the substrates) [39, 40]. Wuppertal researchers suspended a series of niobium samples inside the 5-cell cavity during coating, which they used to evaluate whether the tin, which was supplied from below the vertically-oriented cavity, was being transported sufficiently up to the top of the cavity. They observed that the coating thickness decreased as a function of sample distance from the tin source. They were only able to supply a layer with relatively uniform thickness over all samples by performing a second coating cycle, with the cavity upside down. Preliminary studies were also performed by Wuppertal on a 5-cell 1.5GHz cavity, with similar performance [44]. Future multi-cell coating procedures can develop improved procedures for ensuring a uniform coating over the entire structure, for example through use of higher vapor pressure or distributed tin sources. This may also be beneficial for cavities with complicated endgroup geometry. Figure 25 shows planned apparatuses at Jefferson Lab for coating 5-cell 1.5 GHz cavities with waveguide endgroups

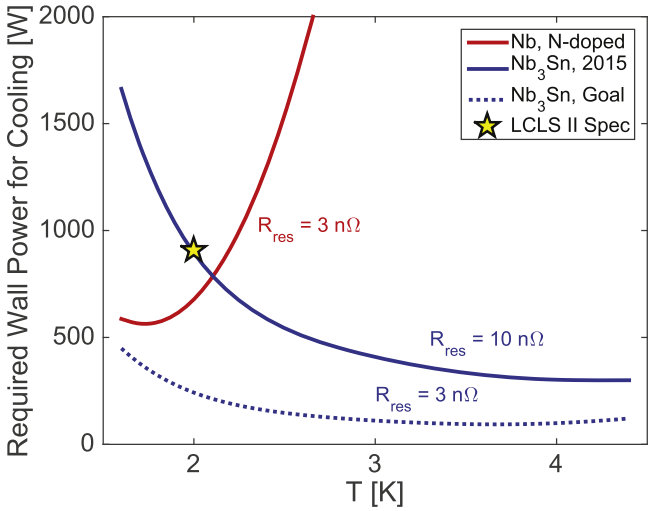

Figure 26. Required power from the grid for removing the heat dissipated by a single cell of a 1.3 GHz cavity at $E_{acc} = 16$ MV m^{-1} as a function of temperature. Calculations of surface resistance are based on previous measurements [79, 81]. For Nb_3Sn, the previously achieved R_{res} of 10 nΩ is plotted, as is a target reduction to 3 nΩ, which has been achieved at low fields [43]. For the same R_{res}, Nb would require significantly more power even when operating at much lower temperatures.

and at Fermilab for coating 1.3 GHz 9-cell and 650 MHz 5-cell cavities.

The thermocurrents observed in Nb_3Sn cavities will require special different precautions in applications. Quench will have to be carefully avoided to prevent strong increase in localized heating. And cavities will have to be carefully cooled slowly and uniformly through the transition temperature to maximize Q_0.

Microphonics compensation will be more challenging when operating substantially above 2 K. Superfluid helium suppresses bubbles, so bubbling will have a more significant impact on the cavity frequency stability at 4.5 K. This can be partially mitigated through engineering of the cavity-helium vessel package to minimize df/dp [104–107]. And of course there are many examples of niobium cavities that successfully operate under the influence of 4.5 K microphonics [108–110].

Finally, the coating technology must be transferred to the industry if it is to be implementation in large-scale production. However, once the procedure has been established at a vendor, the cost per coating is expected to have a relatively small impact relative to the total price for a processed cavity.

6. Conclusion

By far, Nb_3Sn shows the strongest performance of alternative materials being studied for SRF applications, with 1.3 GHz single cell cavity measurements demonstrating both useful gradients and 4.2 K Q_0 values that are similar to 2.0 K Q_0 values for niobium. The operating temperature is significant: at 4.2 K, cryogenic efficiency is 3–4 times higher, and the cryogenic plant is simpler and more reliable. As figure 26 shows, this is expected to provide a substantial cost savings for using SRF cavities with high quality Nb_3Sn coatings in large high duty factor accelerators, including linacs for light sources, nuclear physics, and high energy physics, as well as circular high energy electron positron colliders. There are several practical considerations to work on before Nb_3Sn can be used in applications, but progress is expected with sustained R&D.

CW tests of TM cavities show peak surface magnetic field limitations ~70 mT, but much higher fields are observed in pulsed measurements and in CW measurements and in TE cavities. Limitations are consistent with defects, and pulsed measurements indicate a trend at high temperatures toward the predicted ultimate limiting field, approximately twice as high as niobium. This shows potential for high energy linac applications, and additional research to avoid low tin-content regions may help to increase quench fields.

Nb_3Sn cavities may be especially beneficial in small scale accelerator applications. The ability to operate with high Q_0 at 4.2 K opens the possibility of cooling cavities with a cryocooler, instead of a cryogenic plant, greatly reducing infrastructure cost, subsystem footprint, and labor for operation and maintenance. This could enable new industrial applications for SRF accelerators in medicine, border security, and treatment of flue gas and wastewater. Existing cavities show dissipation within the capacity of cryocoolers [111], and future development is expected to increase quality factors even further.

Acknowledgments

The authors would like to thank previous Nb_3Sn SRF researchers who made possible the ongoing research into this material. Special thanks to Grigory Eremeev, Arno Godeke, Peter Kneisel, Matthias Liepe, Michael Peiniger, and Yulia Trenikhina for contributions and for useful discussions. This work was supported by the United States Department of Energy, Offices of High Energy Physics. Fermilab is operated by Fermi Research Alliance, LLC under Contract No. DE-AC02-07CH11359 with the United States Department of Energy. This work includes results from the Nb_3Sn program at Cornell University, which is lead by P I Matthias Liepe with support from United States Department of Energy grant DE-SC0008431 and United States National Science Foundation PHY-141638. Material included in this work made use of the Cornell Center for Materials Research Shared Facilities, which are supported through the United States National Science Foundation MRSEC program (DMR-1120296).

References

[1] Galayda J N 2015 *LCLS-II Final Design Report* LCLSII-1.1-DR-0251-R0 Linac Coherent Light Source II (LCLS-II) Project

[2] Peggs S 2012 *Conceptual Design Report* ESS-2012-001 European Spallation Source

[3] Altarelli M *et al* 2007 *The European X-Ray Free-Electron Laser Technical design report* DESY 2006-097 DESY http://xfel.desy.de/technical_information/tdr/tdr/

[4] Brüning O S, Collier P, Lebrun P, Myers S, Ostojic R, Poole J and Proudlock P 2004 *LHC Design Report* CERN-2004-003-V-1 CERN http://cds.cern.ch/record/782076/files/

[5] Mason T E *et al* 2006 The spallation neutron source in Oak Ridge: a powerful tool for materials research *Physica* B **385–386** 955–60

[6] Myers S 1990 *The LEP Collider from design to approval and commissioning* CERN 91-08 CERN https://cas.web.cern.ch/cas/John%20Adams'%20Lectures/Myers.pdf

[7] Reece C E 2016 Continuous wave superconducting radio frequency electron linac for nuclear physics research *Phys. Rev. ST Accel. Beams* **19** 124801

[8] Padamsee H, Knobloch J and Hays T 2008 *RF Superconductivity for Accelerators* (New York: Wiley-VCH)

[9] Padamsee H 2009 *RF Superconductivity: Vol II: Science, Technology and Applications* (Weinheim: Wiley-VCH)

[10] Bernard P, Bloess D and Flynn T 1992 Superconducting niobium sputter-coated copper cavities at 1500 MHz *Proc. 3rd European Particle Accelerator Conf.* pp 1269–71

[11] Kneisel P, Lewis B and Turlington L 1993 Experience with high pressure ultrapure water rinsing of niobium cavities *Proc. 6th Workshop on RF Superconductivity*

[12] Proch D and Klein U 1979 Multipacting in superconducting RF structures *Proc. Conf. for Future Possibilities for Electron Accelerators* pp N1–17

[13] Visentin B 1998 R&D issues in superconducting cavities *TESLA Meeting, DESY 98-05*

[14] Kneisel P 1999 Preliminary experience with 'in-situ' baking of niobium cavities *Proc. 9th Workshop on RF Superconductivity* pp 328–35

[15] Bean C P and Livingston J D 1964 Surface barrier in type-II superconductors *Phys. Rev. Lett.* **12.1** 14

[16] Matricon J and Saint-James D 1967 Superheating fields in superconductors *Phys. Lett.* A **24** 241–2

[17] Catelani G and Sethna J P 2008 Temperature dependence of the superheating field for superconductors in the high-κ London limit *Phys. Rev.* B **78** 224509

[18] Liarte D B, Posen S, Transtrum M K, Catelani G, Liepe M and Sethna J P 2017 Theoretical estimates of maximum fields in superconducting resonant radio frequency cavities: stability theory, disorder, and laminates *Supercond. Sci. Technol.* **30** 033002

[19] Geng R L 2006 Review of new shapes for higher gradients *Physica* C **441** 145–50

[20] Furuta F *et al* 2006 Experimental comparison at KEK of high gradient performance of different single cell superconducting cavity designs *EPAC 2006—Contributions to the Proc.* pp 750–2

[21] Valente-Feliciano A-M 2016 Superconducting RF materials other than bulk niobium: a review *Supercond. Sci. Technol.* **29** 113002

[22] Transtrum M K, Catelani G and Sethna J P 2011 Superheating field of superconductors within Ginzburg–Landau theory *Phys. Rev.* B **83** 094505

[23] Schneider W J, Kneisel P and Rode C H 2003 Gradient optimization for SC CW accelerators *Proc. Particle Accelerator Conf. 2003* pp 2863–5

[24] Behnke T, Brau J E, Foster B, Fuster J, Harrison M, Paterson J M, Peskin M, Stanitzki M, Walker N and Yamamoto H 2013 *The International Linear Collider Technical Design Report* ILC-TDR The International Linear Collider https://www.linearcollider.org/ILC/Publications/Technical-Design-Report

[25] Peterson T 2015 personal communication

[26] Hillenbrand B 1980 The preparation of superconducting Nb_3Sn surfaces for RF applications *Proc. 1st Workshop on RF Superconductivity (Karlsruhe)*

[27] Schilcher T 1995 Wärmeleitvermögen von Niob bei kryogenischen temperaturen *PhD Thesis* Universität Regensburg/DESY

[28] Wang Y 2013 *Fundamental Elements of Applied Superconductivity in Electrical Engineering* (Singapore: Wiley)

[29] Godeke A 2006 A review of the properties of Nb_3Sn and their variation with A15 composition, morphology and strain state *Supercond. Sci. Technol.* **19** R68–80

[30] Charlesworth J P, Macphail I and Madsen P E 1970 Experimental work on the niobium–tin constitution diagram and related studies *J. Mater. Sci.* **5** 580–603

[31] Feschotte P, Polikar A and Burri G 1979 Equilibres de phases dans les systemes binaries Nb–Ge et Nb–Sn *C. R. Seances Acad. Sci.* C **288** 125–8

[32] Okamoto H 1990 Nb–Sn (niobium–tin) *Binary Alloy Phase Diagrams* ed T B Massalski (Materials Park, OH: ASM International)

[33] Matthias B T, Geballe T H, Geller S and Corenzwit E 1954 Superconductivity of Nb_3Sn *Phys. Rev.* **95** 1435

[34] Schwettman H A, Wilson P B, Pierce J P and Fairbank W M 1965 The application of superconductivity to electron linear accelerators *Int. Adv. Cryog. Eng.* **10** 88–92

[35] Hillenbrand B, Martens H, Pfister H, Schnitzke K and Ziegler G 1975 Superconducting Nb_3Sn cavities *IEEE Trans. Magn.* **11** 420–2

[36] Saur E and Wurm J 1962 Preparation und Supraleitungseigenschaften von Niobdrahtproben mit Nb_3Sn-Uberzug *Naturwissenschaften* **49** 127–8

[37] Heinrichs H, Grundey T, Minatti N, Muller G, Peiniger M, Piel H, Unterborsch G, Vogel H P and Bergische Universitat-gesamthochschule Wuppertal 1984 Activities on RF-Superconductivity at Wuppertal *Proc. 2nd Workshop on RF Superconductivity (Geneva)*

[38] Boccard P, Kneisel P, Müller G, Pouryamout J and Piel H 1997 Results from some temperature mapping experiments on Nb_3Sn RF cavities *Proc. 8th Workshop on RF Superconductivity (Padova)*

[39] Peiniger M and Piel H 1985 A superconducting Nb_3Sn coated multicell accelerating cavity *IEEE Trans. Nucl. Sci.* **32** 3610–2

[40] Arnolds-Mayer G and Chiaveri E 1986 On a 500 MHz single cell cavity with Nb_3Sn surface *Proc. 3rd Workshop on RF Superconductivity (Chicago)*

[41] Allen L, Beasley M, Hammond R and Turneaure J 1983 RF surface resistance of high-Tc superconducting A15 thin films *IEEE Trans. Magn.* **19** 1003–6

[42] Stimmell J B 1978 Microwave superconductivity of Nb_3Sn *PhD Thesis* Cornell University

[43] Müller G, Piel H, Pouryamout J, Boccard P and Kneisel P 2000 Status and Prospects of Nb_3Sn cavities for superconducting linacs *Proc. Workshop on Thin Film Coating Methods for Superconducting Accelerating Cavities (Hamburg)* ed D Proch TESLA Report 2000-15

[44] Müller G, Kneisel P and Mansen D 1996 Nb_3Sn layers on high-purity Nb cavities with very high quality factors and accelerating gradients *Proc. 8th European Particle Accelerator Conf. (Sitges)*

[45] Posen S and Liepe M 2011 Stoichiometric Nb_3Sn in first samples coated at cornell *Proc. SRF 2011 (Chicago, Illinois)*

[46] Eremeev G, Reece C E, Kelley M J, Pudasaini U and Tuggle J R 2015 Progress with multi-cell Nb_3Sn cavity development linked with sample matierals characterization

Proc. 17th Int. Conf. on RF Superconductivity (Whistler, Canada) p TUBA05
[47] Posen S, Merio M, Alex Romanenko and Trenikhina Y 2015 Fermilab Nb_3Sn R&D Program *Proc. SRF 2015 (Whistler)*
[48] Rosaz G *et al* 2016 Production and R&D thin films activities at CERN for SRF applications *Proc. TeSLA Technology Collaboration Meeting*
[49] Barzi E, Bestetti M, Reginato F, Turrioni D and Franz S 2016 Synthesis of superconducting Nb_3Sn coatings on Nb substrates *Supercond. Sci. Technol.* **29** 015009
[50] Krishnan M 2012 Niobium coatings for SRF cavities produced by high power impulse magnetron sputtering *Proc. 5th Int. Workshop on Thin Films and New Ideas for Pushing the Limits of RF Superconductivity (Newport News)*
[51] Mitsunobu S 2010 Status of KEK studies on MgB_2 *Proc. 4th Int. Workshop on Thin Films and New Ideas for Pushing the Limits of RF Superconductivity (Padua)*
[52] Deambrosis S M, Rampazzo V, Rossi A A, Rupp V, Sharma R G, Stark S, Stivanello F and Palmieri V 2009 A15 superconductors by thermal diffusion in 6 GHz cavities *Proc. SRF 2009 (Berlin)*
[53] Rossi A A, Deambrosis S M, Stark S, Rampazzo V, Rupp V, Sharma R G, Stivanello F and Palmieri V 2009 Nb_3Sn films by multilayer sputtering *Proc. SRF 2009 (Berlin)*
[54] Deambrosis S M, Keppel G, Ramazzo V, Roncolato C, Sharma R G and Palmieri V 2006 A15 superconductors: An alternative to niobium for RF cavities *Physica* C **441** 108–13
[55] Carta G, Rossetto G, Zanella P, Crociani L, Palmieri V and Todescato F 2006 Attempts to deposit Nb_3Sn by MO-CVD *Proc. Int. Workshop on Thin Films and New Ideas for Pushing the Limits of RF Superconductivity (Padua)*
[56] Hammond R 1975 Electron beam evaporation synthesis of A15 superconducting compounds: Accomplishments and prospects *IEEE Trans. Magn.* **11** 201–7
[57] Hakimi M 1988 Bronze-processed Nb_3Sn for RF applications *J. Less Common Metals* **139** 159–65
[58] Hasse J, Hermann W D and Orlich R 1974 On the microwave absorption of superconducting Nb_3Sn *Z. Phys.* **271** 265–8
[59] Perpeet M, Cassinese A, Hein M A, Kaiser T, Muller G, Piel H and Pouryamout J 1999 Nb_3Sn films on sapphire. a promising alternative for superconductive microwave technology *IEEE Trans. Appl. Supercond.* **9** 2496–9
[60] Hillenbrand B, Uzel Y and Schnitzke K 1980 On the preparation of Nb_3Sn-layers on monocrystalline Nb-substrates *Appl. Phys.* **23** 237–40
[61] Dasbach D, Müller G, Peiniger M, Piel H and Roth R W W 1989 and Fachbereich Physik Nb_3Sn coating of high purity Nb cavities *IEEE Trans. Magn.* **25** 1862–4
[62] Peiniger M 1983 Herstellung und Test eines S-Band Resonators mit Nb_3Sn-Oberflache *PhD Thesis* University of Wuppertal
[63] Mucklejohn S A and O'Brien N W 1987 The vapour pressure of tin(II) chloride and the standard molar Gibbs free energy change for formation of $SnCl_2$(g) from Sn(g) and Cl_2(g) *J. Chem. Thermodyn.* **19** 1079–85
[64] Loeb L B 2004 *The Kinetic Theory of Gases* (New York: Dover Publications)
[65] Meurant G 1958 *Advances in Chemical Engineering* vol 2 (Amsterdam: Elsevier)
[66] Hall D L, Gruber T, Kaufman J J, Liepe M, Maniscalco J, Posen S, Yu B and Proslier T 2015 Nb_3Sn cavities: material characterisation and coating process optimisation *Proc. SRF 2015 (Whistler)*
[67] Hillenbrand B 1976 Superconducting Nb_3Sn cavities with high quality factors and high critical flux densities *J. Appl. Phys.* **47** 4151
[68] Martens H, Martens H, Martens R, Martens H-W, Martens G, Martens S, Martens H and Martens H 1978 Method for the manufacture of a superconductive Nb_3Sn layer on a niobium surface for high frequency applications *US Patent* 4,105,512
[69] Arnolds-Mayer G 1984 A15 surfaces in Nb cavities *Proc. 2nd Workshop on RF Superconductivity (Geneva)*
[70] Hillenbrand B, Krause N, Pfister H, Schnitzke K and Uzel Y 1981 *Supraleitende Nb_3Sn resonatoren* BMFT-FB-T 81-188 Siemens AG
[71] Peiniger M, Hein M, Klein N, Müller G, Piel H and Thuns P 1988 Work on Nb_3Sn cavities at Wuppertal *Proc. 3rd Workhop on RF Superconductivity (Argonne National Laboratory)*
[72] Kneisel P, Amato J, Kirchgessner J, Nakajima K, Padamsee H, Phillips H, Reece C, Sundelin R and Tigner M 1985 Performance of superconducting storage ring cavities at 1500 MHz *IEEE Trans. Magn.* **21** 1000–3
[73] Knobloch J 1997 Advanced thermometry studies of superconducting RF cavities *PhD Thesis* Cornell University
[74] Gurevich A 2006 Enhancement of rf breakdown field of superconductors by multilayer coating *Appl. Phys. Lett.* **88** 012511
[75] Hein M 1999 *High-Temperature-Superconductor Thin Films at Microwave Frequencies* (New York: Springer)
[76] Godeke A 2005 Performance boundaries in Nb_3Sn superconductors *PhD Thesis* University of Twente, Enschede, The Netherlands
[77] Orlando T P, McNiff E J, Foner S and Beasley M R 1979 Critical fields, Pauli paramagnetic limiting, and material parameters of Nb_3Sn and V_3Si *Phys. Rev.* B **19** 4545–61
[78] Maxfield B and McLean W 1965 Superconducting penetration depth of niobium *Phys. Rev.* **139** A1515–22
[79] Posen S 2015 Understanding and overcoming limitation mechanisms in Nb_3Sn superconducting RF cavities *PhD Thesis* Cornell University
[80] Hall D L 2016 Next generation Nb_3Sn cavities: current performance, limitations, and considerations for practical use *Presented at the Tesla Technology Collaboration meeting at CEA Saclay (Paris)*
[81] Hall D L, Gruber T, Kaufman J J, Liepe M, Maniscalco J T, Posen S, Yu B and Proslier T 2015 Nb_3Sn cavities: material characterization and coating process optimization *Proc. 17th Int. Conf. on RF Superconductivity*p TUBA04
[82] Halbritter J 1970 FORTRAN-program for the computation of the surface impedance of superconductors *Internal Note KFZ Karlsruhe* 3/70-6
[83] Halbritter J 1970 Comparison between measured and calculated RF losses in the superconducting state *Z. Phys.* **238** 466–76
[84] Valles N R A 2014 Pushing the frontiers of superconducting radio frequency science: from the temperature dependence of the superheating field of niobium to higher-order mode damping in very high quality factor accelerating structures *PhD Thesis* Cornell University
[85] Meyers S, Posen S and Liepe M 2014 Analysis of systematic and random error in SRF material parameter calculations *Proc. 27th Linear Accelerator Conf.*
[86] Campisi I 1985 High field RF superconductivity: To pulse or not to pulse? *IEEE Trans. Magn.* **21** 134–41
[87] Hays T and Padamsee H 1997 Measuring the RF critical field of Pb, Nb, and Nb_3Sn *Proc. 8th Workshop on RF Superconductivity (Padova)* pp 789–94
[88] Posen S, Valles N and Liepe M 2015 Radio frequency magnetic field limits of Nb and Nb_3Sn *Phys. Rev. Lett.* **115** 047001
[89] Kneisel P, Stoltz O and Halbritter J 1979 Measurements of superconducting Nb_3Sn cavities in the GHz range *IEEE Trans. Magn.* **15** 21–4

[90] Bonin B and Safa H 1991 Power dissipation at high fields in granular RF superconductivity *Supercond. Sci. Technol.* **4** 257–261
[91] Perpeet M, Hein M A, Muller G, Piel H, Pouryamout J and Diete W 1997 High-quality Nb_3Sn thin films on sapphire prepared by tin vapor diffusion *J. Appl. Phys.* **82** 5021
[92] Romanenko A, Grassellino A, Crawford A C, Sergatskov D A and Melnychuk O 2014 Ultra-high quality factors in superconducting niobium cavities in ambient magnetic fields up to 190 mG *Appl. Phys. Lett.* **105** 234103
[93] Peiniger M 1989 Experimental investigations on superconducting Nb_3Sn-cavities at microwave frequencies *PhD Thesis* University of Wuppertal Report WUB-DIS 89-1
[94] Old C F and Macphall I 1969 The mechanism and kinetics of growth of the superconducting compound Nb_3Sn *J. Mater. Sci.* **4** 202–7
[95] Farrell H H 1974 Grain boundary diffusion and growth of intermetallic layers: Nb_3Sn *J. Appl. Phys.* **45** 4025
[96] Hillenbrand B, Martens H, Pfister H, Schnitzke K and Uzel Y 1977 Superconducting Nb_3Sn cavities with high microwave qualities *IEEE Trans. Magn.* **13** 491–5
[97] Tuggle J, Eremeev G V, Reece C E, Xu H and Kelley M J 2015 Structure and composition of Nb_3Sn diffusion coated films on Nb *Proc. SRF 2015 (Whistler)*
[98] Becker C, Posen S, Groll N, Cook R, Schlepütz C M, Hall D L, Liepe M, Pellin M, Zasadzinski J and Proslier T 2015 Analysis of Nb_3Sn surface layers for superconducting radio frequency cavity applications *Appl. Phys. Lett.* **106** 082602
[99] Posen S, Melnychuk O, Romanenko A, Sergatskov D, Leslie Hall D and Liepe M 2015 Cutout study of a Nb_3Sn cavity *Proc. SRF 2015 (Whistler)*
[100] Hall D L, Kaufman J J, Liepe M and Maniscalco J 2016 Surface analysis studies of Nb_3Sn thin films *Proc. IPAC 2016 (Busan)*
[101] Hall D L, Liepe M and Maniscalco J 2016 RF measurements on high performance Nb_3Sn cavities *Proc. IPAC 2016 (Busan)*
[102] Reece C, Eremeev G, Pudasaini U, Tuggle J R and Kelley M J 2016 Nb_3Sn developments at JLab *TeSLA Technology Collaboration Meeting*
[103] Aull S, Junginger T, Knobloch J and Neupert H 2015 Secondary electron yield of SRF materials *Proc. 17th Int. Conf. on RF Superconductivity (Whistler, Canada)* p TUPB050
[104] Shepard K W, Kelly M P, Fuerst J D, Kedzie M and Conway Z A 2005 Superconducting triple-spoke cavity for beta=0.5 ions *Proc. 2005 Particle Accelerator Conf.* (Piscataway, NJ: IEEE) pp 4344–6
[105] Zaplatin E, Compton C, Hartung W, Johnson M J, Marti F, Oliva J, Popielarski J and York R C 2009 Structural analysis of MSU quarter-wave resonators *Proc. 14th Conf. on RF Superconductivity* pp 560–3
[106] Posen S and Liepe M 2012 Mechanical optimization of superconducting cavities in continuous wave operation *Phys. Rev. ST Accel. Beams* **15** 022002
[107] Passarelli D, Awida M H, Gonin I V, Ristori L, Yakovlev V P and Dottorato L 2012 Pressure sensitivity characterization of superconducting spoke cavities *Proc. 3rd Int. Particle Accelerator Conf.* (2–4 May)
[108] Padamsee H *et al* 1991 Accelerating cavity development for the Cornell B-factory, CESR-B *Particle Accelerator Conf. 1991* vol 2, pp 786–8
[109] Benvenuti C 1991 Superconducting coatings for accelerating RF cavities: past, present, future *Proc. 5th Workshop on RF Superconductivity*
[110] Boussard D, Chiaveri E, Haebel E, Kindermann H P, Losito R, Marque S, Rodel V and Stirbet M 1999 The LHC superconducting cavities *Proc. 1999 Particle Accelerator Conf. (Cat. No.99CH36366)* vol 2, pp 946–8
[111] 2012 Cryocooler product catalogue pp 1–20, Sumitomo Heavy Industries http://www.shicryogenics.com/wp-content/uploads/2012/11/Cryocooler-Product-Catalogue.pdf